nature climate change

LETTERS

PUBLISHED ONLINE: 29 JUNE 2015 | DOI: 10.1038/NCLIMATE2688

Decreasing intensity of open-ocean convection in the Greenland and Iceland seas

G. W. K. Moore[1]*, K. Våge[2], R. S. Pickart[3] and I. A. Renfrew[4]

The air–sea transfer of heat and fresh water plays a critical role in the global climate system[1]. This is particularly true for the Greenland and Iceland seas, where these fluxes drive ocean convection that contributes to Denmark Strait overflow water, the densest component of the lower limb of the Atlantic Meridional Overturning Circulation (AMOC; ref. 2). Here we show that the wintertime retreat of sea ice in the region, combined with different rates of warming for the atmosphere and sea surface of the Greenland and Iceland seas, has resulted in statistically significant reductions of approximately 20% in the magnitude of the winter air–sea heat fluxes since 1979. We also show that modes of climate variability other than the North Atlantic Oscillation (NAO; refs 3–7) are required to fully characterize the regional air–sea interaction. Mixed-layer model simulations imply that further decreases in atmospheric forcing will exceed a threshold for the Greenland Sea whereby convection will become depth limited, reducing the ventilation of mid-depth waters in the Nordic seas. In the Iceland Sea, further reductions have the potential to decrease the supply of the densest overflow waters to the AMOC (ref. 8).

Sea ice in the Iceland and Greenland seas has undergone pronounced fluctuations since 1900 (ref. 9; Fig. 1). In particular, the early twentieth century warming period from the 1920s to the 1940s (ref. 10) was characterized by reduced ice extent, whereas there was an expansion of sea ice during the mid-century cooling period from the 1960s to the 1970s (ref. 11). The reduction in sea ice concentration that has occurred over the past 30 years is unprecedented in this 111-year-long record and has resulted in the lowest sea-ice extent in the region since the 1200s (ref. 12).

The Iceland and Greenland seas contain gyres (Fig. 1) where oceanic convection occurs[8,13,14], a process that is crucial for dense water formation, and thus the AMOC (refs 8,13). Open-ocean convection requires a suitably preconditioned environment, typically a cyclonic gyre which domes the isopycnals, resulting in a weakly stratified mid-depth water column. This makes it easier for convective overturning to extend to greater depths once the surface waters lose buoyancy through the transfer of heat and moisture to the atmosphere[13]. The buoyancy loss tends to be largest at the ice edge, where cold and dry Arctic air first comes into contact with the relatively warm surface waters[15]. The recent retreat of wintertime sea ice (Fig. 1) has increased the distance of these two oceanic gyres from the ice edge—and, hence, the region of largest heat loss. Here we address how this change is affecting ocean convection.

We focus on the changes in winter-mean conditions for the period 1958–2014, using a merged data set, described in the Supplementary Methods, consisting of the 40-year (ERA-40) and the Interim (ERA-I) Reanalyses, both from the European Centre for Medium-Range Weather Forecasts[16,17]. As can be seen from Fig. 1, this time period covers both the mid-century cooling, in which there was an expansion of sea ice in the vicinity of both convection sites, as well as the more recent period with an unprecedented retreat of ice across the entire region.

Figure 2 shows the winter-mean sea-ice concentration within the two gyres, as well as the turbulent heat flux $Q_{\mathrm{thf}}^{\mathrm{ocean}}$ within the open-water portion of the gyres (error estimates described in the Supplementary Methods). Consistent with Fig. 1, both gyres had their highest sea-ice concentrations in the late 1960s. Since that time, sea-ice cover in the Iceland Sea gyre has vanished, whereas in the Greenland Sea gyre it persisted until the mid-1990s, after which it also disappeared. The time series of $Q_{\mathrm{thf}}^{\mathrm{ocean}}$ shows that both gyres are subject to considerable inter-annual variability in atmospheric forcing as well as long-term tendencies towards reduced fluxes. This low-frequency variability has been assessed using singular spectrum analysis (SSA), a non-parametric spectral analysis technique that uses data-adaptive basis functions to partition a time series into components that maximize the described variability in the original time series[18]. For the Iceland Sea site, the low-frequency SSA reconstruction indicates that there has been a steady reduction in $Q_{\mathrm{thf}}^{\mathrm{ocean}}$ since the time of the region's sea-ice maximum in the late 1960s. For the Greenland Sea site, the reconstruction indicates that the period of interest is characterized by small-amplitude multi-decadal variability, with a trend towards lower values that began in the mid-1990s, and which coincides with the onset of ice-free conditions in the gyre. As shown in Fig. 1, there is nevertheless still sea ice present to the northwest of both gyres.

As discussed in the Supplementary Methods, the correlation of $Q_{\mathrm{thf}}^{\mathrm{ocean}}$ over both gyres with the winter-mean index of the NAO, the leading mode of climate variability in the North Atlantic[4], is not statistically significant. This suggests, in agreement with previous studies[7,19], that modes of variability other than the NAO are needed to fully describe the climate in the region.

Piecewise continuous linear least-squares fits to $Q_{\mathrm{thf}}^{\mathrm{ocean}}$ at both sites with breakpoints consistent with the SSA low-frequency behaviour (1970 for the Iceland Sea and 1992 for the Greenland Sea) are also shown in Fig. 2. At both sites, the trends after the breakpoints are statistically significant at the 95th percentile confidence interval. As described in the Supplementary Methods, all significance tests presented here take into account the 'red noise' characteristic of geophysical time series. Indeed, since 1979 there has been a reduction in the magnitude of $Q_{\mathrm{thf}}^{\mathrm{ocean}}$ over both gyres of approximately 20%. Similar results hold if one includes the net radiative flux to obtain the total heat flux over the open ocean (Supplementary Fig. 1).

[1]Department of Physics, University of Toronto, Toronto, Ontario M5S A17, Canada. [2]Geophysical Institute, University of Bergen and Bjerknes Centre for Climate Research, Bergen 5020, Norway. [3]Department of Physical Oceanography, Woods Hole Oceanographic Institution, Woods Hole, Massachusetts 02543-1050, USA. [4]Centre for Ocean and Atmospheric Sciences, School of Environmental Sciences University of East Anglia, Norwich NR4 7TJ, UK. *e-mail: gwk.moore@utoronto.ca

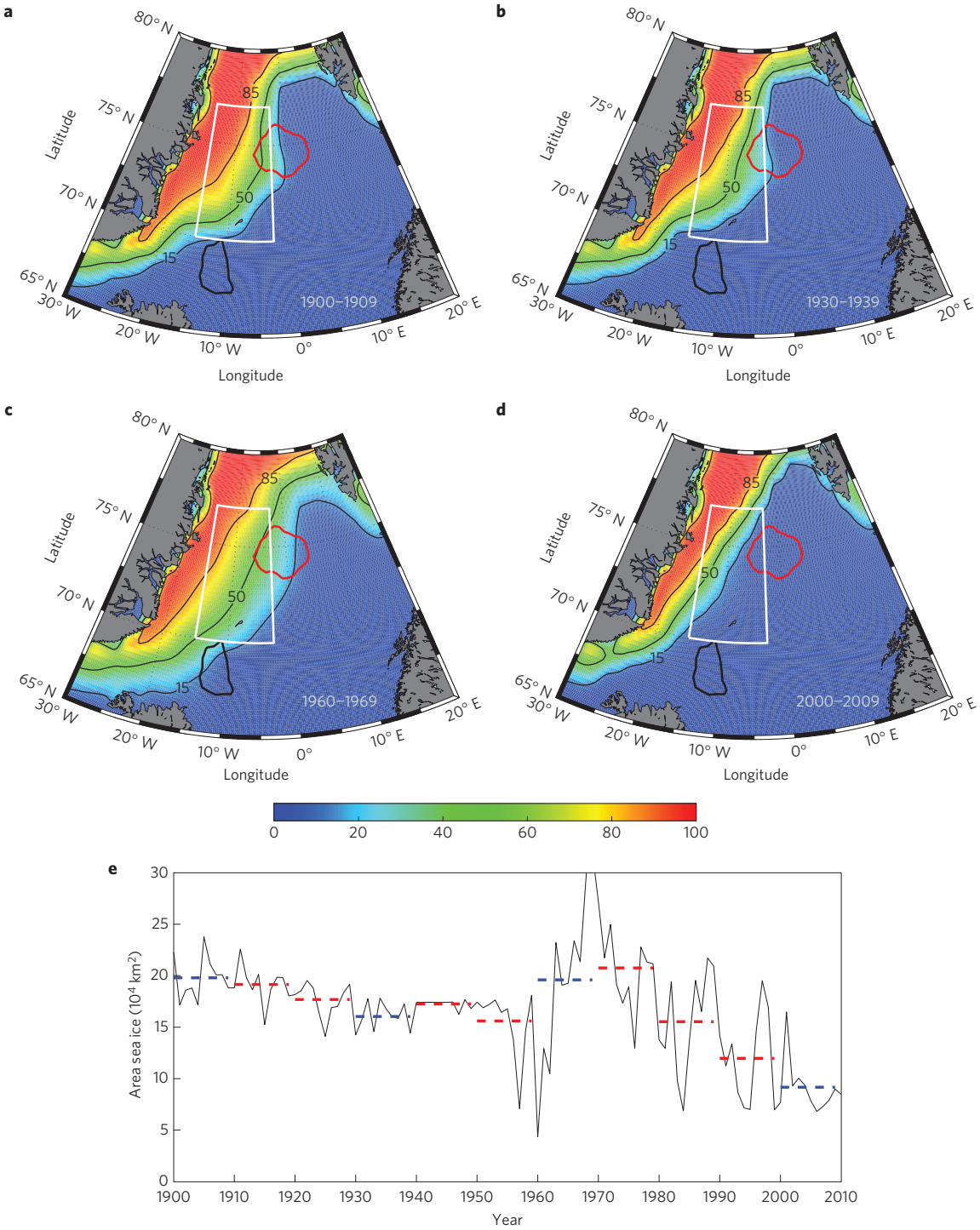

Figure 1 | Winter sea-ice extent for the Nordic seas. a–d, Four decadal mean maps of sea-ice concentration (%) for 1900–1909 (**a**), 1930–1939 (**b**), 1960–1969 (**c**) and 2000–2009 (**d**). **e**, Time series of winter-mean sea ice area for the region indicated by the white boxes in **a–d** for the period 1900–2010. The decadal means for the periods shown in **a–d** are in blue with the other decadal means in red. In **a–d**, the gyres in the Iceland and Greenland seas where oceanic convection occurs are indicated by the thick black and red curves, respectively.

The turbulent heat flux $Q_{\mathrm{thf}}^{\mathrm{ocean}}$ is the sum of the sensible and latent heat fluxes. These components tend to be spatially similar, and, in this region, the sensible heat flux usually dominates[6]. The sensible heat flux is parameterized as being proportional to the product of the 10 m wind speed and the air–sea temperature difference[20]. The time series of the latter, as well as their low-frequency SSA reconstructions over the two convection sites, are also shown in Fig. 2 and indicate a tendency for a reduced air–sea temperature difference in recent years over both sites. This is due to the atmosphere warming at a faster rate than the ocean, thus leading to a reduction in $Q_{\mathrm{thf}}^{\mathrm{ocean}}$. Figure 2 indicates that there has been a recent reduction in the 10 m wind speed over the Iceland Sea that is also contributing to the $Q_{\mathrm{thf}}^{\mathrm{ocean}}$ trend. In contrast, the 10 m wind speeds over the Greenland Sea indicate the presence of multi-decadal variability, but no trend.

Unfortunately there are no suitably long oceanographic time series with which to document the oceanic response to this

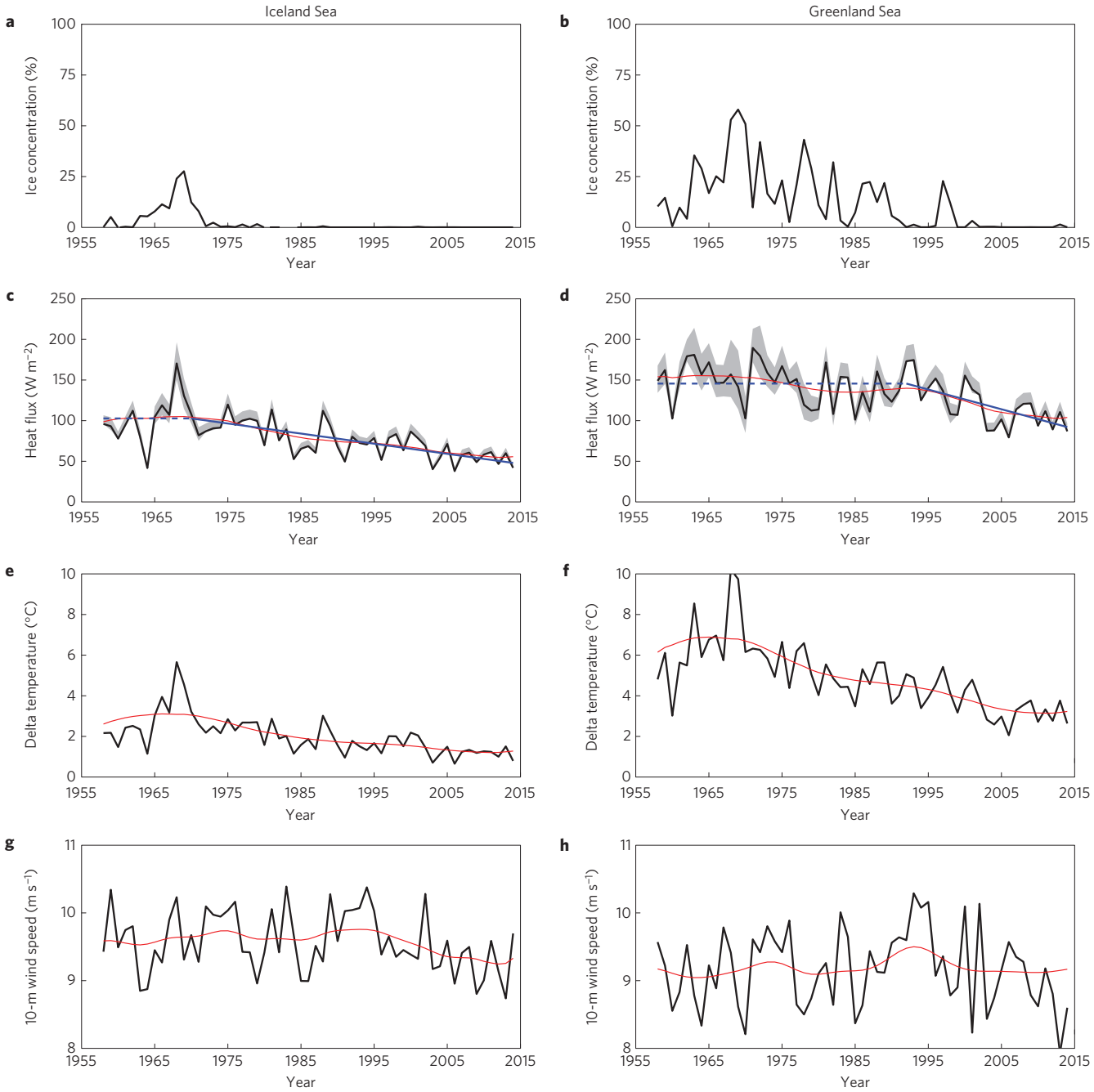

Figure 2 | Time series of the winter-mean conditions over the Iceland and Greenland sea gyres. a,**b**, Sea-ice concentration. **c**,**d**, Open-ocean turbulent heat flux, with the shading representative of the uncertainty associated with the sea-ice concentration. **e**,**f**, Air–sea temperature difference. **g**,**h**, 10-m wind speed. The red curves are the SSA reconstructions of the low-frequency variability in the time series, whereas the blue dashed lines in **c** and **d** are continuous piecewise linear least-squares fits. The trend lines that are solid are statistically significant at the 95% confidence level.

reduction in the atmospheric forcing over the Greenland and Iceland seas. As such, we employ a one-dimensional mixed-layer model, known as the PWP model[21], to simulate the wintertime evolution of the mixed-layer in the two gyres under various forcing conditions (see the Supplementary Methods for details). Initial conditions for the PWP model are specified using a collection of October and November hydrographic profiles from within the gyres, obtained from the NISE (ref. 22) database and the Argo profiling float programme over the period 1980 to present (Fig. 3).

The autumn hydrographic profiles reveal that, near the surface, there is substantial variability which rapidly decreases with depth (Fig. 3a,b). The variability is more pronounced in the Greenland Sea, but, in the mean, the density in the upper part of the water column is greater in the Greenland Sea than in the Iceland Sea. Below ~700 m the situation is reversed and the Iceland Sea is more dense (Fig. 3c). Local ventilation in the Iceland Sea does not reach these depths, so the waters there were formed upstream in either the Greenland Sea or the Arctic Ocean, and subsequently spread into the Iceland Sea[14]. More recently formed intermediate waters in the Greenland Sea (after the cessation of bottom water production there[23]) are less dense. As a result of these factors, the upper ~1,500 m of the Greenland Sea is less stratified than the Iceland Sea. This, together with the substantially higher heat fluxes of the Greenland Sea (Fig. 2), are the major contributors to

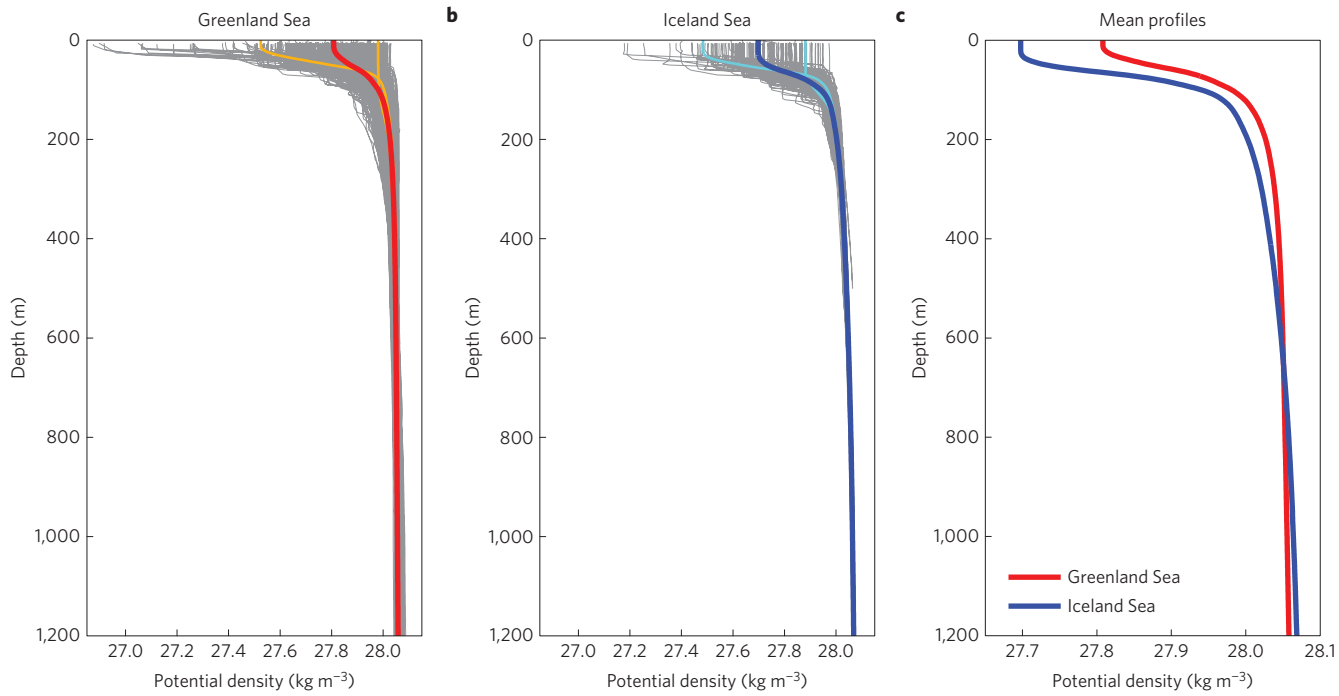

Figure 3 | Potential density profiles for October and November used as initial conditions for the PWP model. a,**b**, Profiles for the Greenland Sea (**a**) and the Iceland Sea (**b**). The traces are individual profiles (grey), means of the 20% most- and least-stratified profiles (orange and cyan), and overall means (red and blue). **c**, Comparison of the mean profile from each gyre. Note the different *x*-axis scale.

deeper convection within the Greenland Sea gyre as compared to the Iceland Sea gyre[13].

To gauge the effectiveness of the PWP model, we used the Argo data to identify a weak (2012) and a strong (2008) convective year in the Nordic seas. Using the November hydrographic profiles for individual Argo floats as initial conditions, we compared the evolution of the mixed-layer depth (MLD) in the model (forced by six-hourly atmospheric fluxes from the ERA-I reanalysis product) against the float observations in each gyre (Supplementary Fig. 2). The results are qualitatively comparable, given the stochastic nature of convection, and indicate that the model is able to capture the seasonal evolution of the mixed-layer in both regions as well as its inter-annual variability.

Using a range of initial conditions, we investigated the sensitivity of convection in the Greenland and Iceland seas to the atmospheric forcing (Fig. 4). In particular, we calculated the maximum late-winter MLD attained in each gyre using the mean autumn hydrographic profiles as initial conditions (Fig. 3c) and a prescribed constant atmospheric forcing over the entire winter period from 1 November to 30 April. We note that these constant levels of forcing are idealized and do not take into account synoptic-scale high-heat-flux events[15], which can impact the wintertime evolution of the mixed-layer[24]. Tests with more realistic six-hourly forcing generally produced slightly deeper mixed-layers, but were comparable to those from the corresponding constant-forcing simulations.

Our model results confirm that the likelihood of deep convection is much higher in the Greenland Sea. For example, the maximum model MLD, for the largest observed mean winter forcing, is 1,000 m in the Greenland Sea versus only 500 m in the Iceland Sea. The model results also reveal an unanticipated difference in the behaviour of oceanic convection between the gyres. In the Iceland Sea there is a nearly linear relationship between the maximum MLD and the winter-mean heat flux, throughout the range of forcing (~5 m change in MLD for every 1 W m^{-2}). In contrast, the Greenland Sea is characterized by two distinct convective regimes. For atmospheric forcing less than about 150 W m^{-2}, the MLD increases only moderately with heat flux (~3 m change in MLD for every 1 W m^{-2}). However, for heat fluxes exceeding this value, the MLD is significantly more sensitive to the forcing (~10 m change in MLD for every 1 W m^{-2}). This threshold behaviour is due to the background stratification of the Greenland Sea (Fig. 3). Consequently, if the winter is sufficiently severe to erode the stratification of the upper layer, the weakly stratified waters below the pycnocline present little resistance to deeper convection.

Over the past 30 years the range of mean wintertime atmospheric forcing falls within both of these convective regimes for the Greenland Sea, and shallow as well as deep mixed-layers have been observed and simulated (for example, Supplementary Fig. 2). However, taking into consideration the negative trend of atmospheric forcing documented above (Fig. 2), which is also illustrated by the reduced mean of the 1997–2014 period relative to the 1979–1996 period (see Fig. 4), the Greenland Sea may be undergoing a transition from a state of intermediate depth convection to one in which only shallow convection occurs. If this trend continues, the production of intermediate waters in the Greenland Sea, and hence the ventilation of a substantial volume of the Nordic seas, may be at stake. In the Iceland Sea, the nearly linear convective regime implies a more gradual reduction in convective depth. However, if the decrease in wintertime atmospheric forcing in this region (already 20% smaller than 30 years ago) continues, it will weaken the overturning loop that feeds the North Icelandic Jet[8], thus reducing the supply of the densest water to the AMOC. A measurement system now in place in the Denmark Strait should be able to measure any such changes in properties of the overflow water.

Observations, proxies and model simulations suggest that a recent weakening of the AMOC has occurred[25,26]. Furthermore, models predict that such a slowdown will continue as a result of increasing greenhouse gas concentrations[26,27]. Such a weakening of the AMOC would have drastic impacts on the climate of the North Atlantic and western Europe[28]. Although there is considerable debate regarding the dynamics of the AMOC (ref. 29), one proposed mechanism for its present and predicted decline is a freshening of the

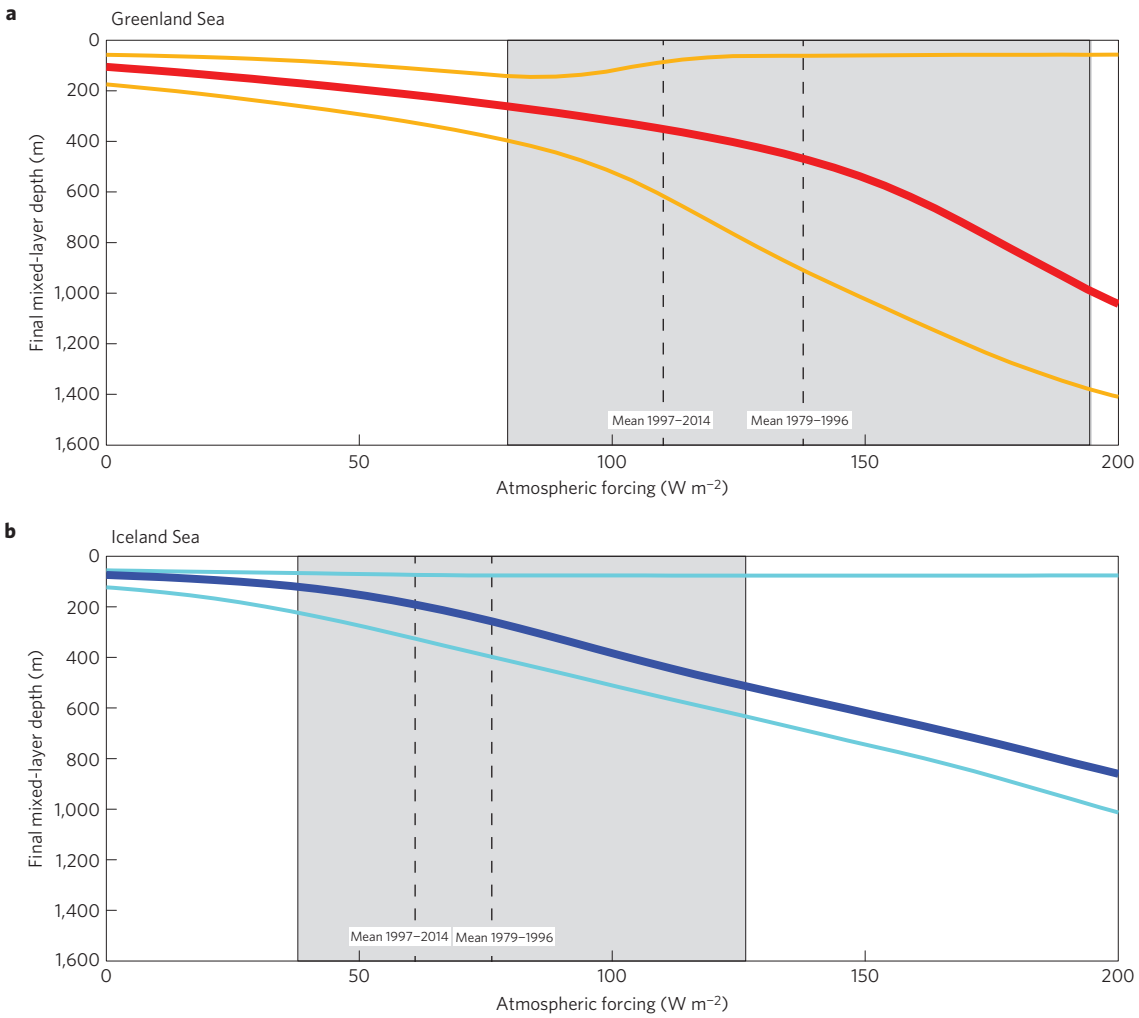

Figure 4 | Relationship between end-of-winter simulated mixed-layer depths from the PWP model and the atmospheric forcing as represented by the winter-mean open-ocean turbulent heat flux. a, Greenland Sea gyre. **b**, Iceland Sea gyre. The thick red (blue) curve shows the final mixed-layer depths resulting from the mean initial conditions, and the thin orange (cyan) curves show the final mixed-layer depths resulting from the strongly and weakly stratified initial conditions. The shaded areas indicate the ranges of winter-mean atmospheric forcing for the period 1979–2014, whereas the dashed lines represent the mean atmospheric forcing for the periods 1979–1996 and 1997–2014.

surface waters—for instance, due to enhanced meltwater emanating from the Greenland Ice Sheet—that reduces their density, making it more difficult for oceanic convection to occur[26,27]. However, much of the freshwater discharge from the Greenland Ice Sheet is apt to be exported equatorwards via the boundary current system surrounding Greenland[30], with limited direct spreading into the interior basins adjacent to the ice sheet where oceanic convection occurs. Further work is thus necessary to determine how and where—and on what timescales—this fresh water pervades the northwest Atlantic. Our results suggest that other possible mechanisms for such a slowdown in the AMOC may be at work; such as a reduction in the magnitude of the surface heat fluxes that trigger the overturning.

Received 25 February 2015; accepted 20 May 2015; published online 29 June 2015

References

1. Curry, J. A. *et al.* Seaflux. *Bull. Am. Meteorol. Soc.* **85,** 409–424 (2004).
2. Mauritzen, C. Production of dense overflow waters feeding the North Atlantic across the Greenland-Scotland Ridge.1. Evidence for a revised circulation scheme. *Deep-Sea Res. I* **43,** 769–806 (1996).
3. Dickson, B. From the Labrador Sea to global change. *Nature* **386,** 649–650 (1997).
4. Hurrell, J. W. Decadal trends in the North-Atlantic Oscillation—regional temperatures and precipitation. *Science* **269,** 676–679 (1995).
5. Jahnke-Bornemann, A. & Bruemmer, B. The Iceland-Lofotes pressure difference: Different states of the North Atlantic low-pressure zone. *Tellus A* **61,** 466–475 (2009).
6. Moore, G. W. K., Renfrew, I. A. & Pickart, R. S. Spatial distribution of air–sea heat fluxes over the sub-polar North Atlantic Ocean. *Geophys. Res. Lett.* **39,** L18806 (2012).
7. Moore, G. W. K., Renfrew, I. A. & Pickart, R. S. Multidecadal mobility of the North Atlantic oscillation. *J. Clim.* **26,** 2453–2466 (2013).
8. Våge, K. *et al.* Significant role of the North Icelandic Jet in the formation of Denmark Strait overflow water. *Nature Geosci.* **4,** 723–727 (2011).
9. Titchner, H. A. & Rayner, N. A. The Met Office Hadley Centre Sea Ice and Sea Surface Temperature Data Set, version 2: 1. Sea ice concentrations. *J. Geophys. Res.* **119,** 2864–2889 (2014).
10. Bengtsson, L., Semenov, V. A. & Johannessen, O. M. The early twentieth-century warming in the Arctic - A possible mechanism. *J. Clim.* **17,** 4045–4057 (2004).
11. Shindell, D. & Faluvegi, G. Climate response to regional radiative forcing during the twentieth century. *Nature Geosci.* **2,** 294–300 (2009).
12. Fauria, M. M. *et al.* Unprecedented low twentieth century winter sea ice extent in the Western Nordic Seas since AD 1200. *Clim. Dynam.* **34,** 781–795 (2010).
13. Marshall, J. & Schott, F. Open-ocean convection: Observations, theory, and models. *Rev. Geophys.* **37,** 1–64 (1999).
14. Swift, J. H., Aagaard, K. & Malmberg, S. A. Contribution of the Denmark Strait overflow to the deep North-Atlantic. *Deep-Sea Res. A* **27,** 29–42 (1980).

15. Renfrew, I. A. & Moore, G. W. K. An extreme cold-air outbreak over the Labrador Sea: Roll vortices and air–sea interaction. *Mon. Weath. Rev.* **127,** 2379–2394 (1999).
16. Uppala, S. M. *et al.* The ERA-40 re-analysis. *Q. J. R. Meteorol. Soc.* **131,** 2961–3012 (2005).
17. Dee, D. P. *et al.* The ERA-Interim reanalysis: Configuration and performance of the data assimilation system. *Q. J. R. Meteorol. Soc.* **137,** 553–597 (2011).
18. Ghil, M. *et al.* Advanced spectral methods for climatic time series. *Rev. Geophys.* **40,** 1003 (2002).
19. Kelly, P. M., Goodess, C. M. & Cherry, B. S. G. The interpretation of the Icelandic sea ice record. *J. Geophys. Res.* **92,** 10835–10843 (1987).
20. Renfrew, I. A., Moore, G. W. K., Guest, P. S. & Bumke, K. A comparison of surface layer and surface turbulent flux observations over the Labrador Sea with ECMWF analyses and NCEP reanalyses. *J. Phys. Oceanogr.* **32,** 383–400 (2002).
21. Price, J. F., Weller, R. A. & Pinkel, R. Diurnal cycling: Observations and models of the upper ocean response to diurnal heating, cooling, and wind mixing. *J. Geophys. Res.* **91,** 8411–8427 (1986).
22. Nilsen, J. E. Ø., Hatun, H., Mork, K. A. & Valdimarsson, H. *The NISE Data Set* (Faroese Fisheries Laboratory, 2008).
23. Ronski, S. & Budeus, G. Time series of winter convection in the Greenland Sea. *J. Geophys. Res.* **110,** C04015 (2005).
24. Våge, K., Pickart, R. S., Moore, G. W. K. & Ribergaard, M. H. Winter mixed-layer development in the central Irminger Sea: The effect of strong, intermittent wind events. *J. Phys. Oceanogr.* **38,** 541–565 (2008).
25. Smeed, D. A. *et al.* Observed decline of the Atlantic meridional overturning circulation 2004–2012. *Ocean Sci.* **10,** 29–38 (2014).
26. Rahmstorf, S. *et al.* Exceptional twentieth-century slowdown in Atlantic Ocean overturning circulation. *Nature Clim. Change* **5,** 475–480 (2015).
27. Wood, R. A., Keen, A. B., Mitchell, J. F. B. & Gregory, J. M. Changing spatial structure of the thermohaline circulation in response to atmospheric CO_2 forcing in a climate model. *Nature* **399,** 572–575 (1999).
28. Bryden, H. L., Longworth, H. R. & Cunningham, S. A. Slowing of the Atlantic meridional overturning circulation at 25° N. *Nature* **438,** 655–657 (2005).
29. Kuhlbrodt, T. *et al.* On the driving processes of the Atlantic meridional overturning circulation. *Rev. Geophys.* **45,** RG2001 (2007).
30. Sutherland, D. A. & Pickart, R. S. The East Greenland Coastal Current: Structure, variability, and forcing. *Prog. Oceanogr.* **78,** 58–77 (2008).

Acknowledgements

The authors would like to thank the European Centre for Medium-Range Weather Forecasts for access to the ERA-40 and ERA-I reanalyses. G.W.K.M. was supported by the Natural Sciences and Engineering Research Council of Canada. K.V. has received funding from NACLIM, a project of the European Union 7th Framework Programme (FP7 2007–2013) under grant agreement no. 308299, and from the Research Council of Norway under grant agreement no. 231647. R.S.P. was supported by the US National Science Foundation. I.A.R. has received funding from the Natural Environmental Research Council for the ACCACIA project (NE/I028297/1).

Author contributions

G.W.K.M., K.V., R.S.P. and I.A.R. jointly conceived the study. G.W.K.M. analysed the atmospheric reanalyses and sea-ice data sets. K.V. carried out the ocean mixed-layer modelling. All authors jointly interpreted the results and wrote the manuscript.

Additional information

Supplementary information is available in the online version of the paper. Reprints and permissions information is available online at www.nature.com/reprints. Correspondence and requests for materials should be addressed to G.W.K.M.

Competing financial interests

The authors declare no competing financial interests.

nature climate change

SUPPLEMENTARY INFORMATION

DOI: 10.1038/NCLIMATE2688

Decreasing intensity of open-ocean convection in the Greenland and Iceland seas

G.W.K. Moore, K. Våge, R.S. Pickart, I.A. Renfrew

1. Reanalyses data

The representation of winter (defined here as the period from 1 November to 30 April) air-sea interaction in the Greenland and Iceland Seas is based on fields from the ERA-40 Reanalysis[31] and the Interim Reanalysis from the ECMWF (ERA-I)[32]. The former covers the period from 1958-2002, while the latter covers the period from 1979-2014. The two share a common lineage, and, not surprisingly, during the period of overlap the correlation coefficient between surface meteorological fields over the Greenland and Iceland Sea gyres was greater than 0.9. For the air-sea heat fluxes, the root-mean-square errors were typically less than 10 W/m^2. To generate continuous time series that span the period from 1958 to the present, we employed a simple merging technique. The ERA-40 data was used for the period 1958-1978; the ERA-I data was used for the period from 1990 onwards; and for 1979-1989, a linear combination was used with the ERA-40 weighting decreasing from 1 to 0 over this period, and the ERA-I weighting increasing from 0 to 1. A small offset of ~5% equal to the difference in the respective means for the overlap period, was also added to the ERA-40 variables in the period 1958-1989 to minimize discontinuities.

2. Air-sea fluxes over sea ice

The transfer of heat and moisture across the air-sea interface are turbulent processes that are mediated by the presence of boundary layer eddies of various scales[33] .

In simplest terms, this transfer is a function of the surface wind speed and the air-sea temperature difference, for the sensible heat flux, and the air-sea humidity difference, for the latent heat or evaporative flux[34]. Higher wind speeds and larger air-sea temperature and humidity differences result in higher heat fluxes[33,35]. There is also typically a large gradient in these fluxes as one transitions from the ice covered regions, where the insulative properties of the ice reduce their magnitude, across the marginal ice zone to the open water[33,35,36]. As a result, the largest heat fluxes occur just downstream of the sea ice cover where the wind speeds are increased due to a reduction in the surface roughness across the marginal ice zone and where the air-sea temperature difference is largest[36,37]. Farther downstream, there is a reduction in the magnitude of the fluxes as the heating and moistening of the boundary layer acts to reduce the air-sea gradients of temperature and moisture[33].

In regions where sea ice is present, the fluxes that are archived in the ECMWF Reanalyses are a weighted sum of the respective fluxes into the atmosphere over open water and sea ice[38]. The insulative character of sea ice significantly reduces the transfer of heat between the atmosphere and ocean, and, as a result, the heat fluxes over sea ice are typically an order of magnitude smaller than the corresponding fluxes over open water[39]. Therefore to estimate the turbulent heat flux that the ocean experiences in partially ice covered regions, the following approach was used. By definition:

$$Q_{thf} = AQ_{thf}^{ice} + (1-A)Q_{thf}^{ocean},$$

$where: Q_{thf}$ is the total turbulent heat flux for that grid point as archived,

A is the sea ice concentration, and

Q_{thf}^{ocean} and Q_{thf}^{ice} are the turbulent heat fluxes over the open ocean and sea ice covered portions of the grid point.

Assuming that $Q_{thf}^{ice} \ll Q_{thf}^{ocean}$, then:

$$Q_{thf}^{ocean} \approx Q_{thf} / (1-A).$$

An estimate of the uncertainty in Q_{thf}^{ocean} was generated by perturbing A by $\pm 10\%$.

The impact that sea ice has on the downstream air-sea heat fluxes can be seen in Supplementary Figure 2 which shows the spatial correlation field of the winter mean sea ice concentration with Q_{thf}^{ocean} averaged over each of the two gyres. In both instances there is a large region of statistically significant positive correlation to the north and west of the respective convection sites, confirming the important role of upwind sea ice for air-sea interaction over these sites. Note that the magnitude of the correlation is higher for the Iceland Sea gyre (>0.6), than for the Greenland Sea gyre (>0.3); this may be the result of the higher variability in sea ice concentration (and more recent sea ice retreat) in the vicinity of the Greenland Sea gyre (Figs. 1-2) or possibly due to more complex air-sea interaction in this region.

3. Assessment of the statistical significance of trends and correlations

Time series of geophysical phenomenon are often characterized by serial auto-correlation or 'red noise'[40]. This leads to a reduction in the degrees of freedom associated with a particular time series that can have an impact on the significance of trends and correlations[41] To take this into account, the statistical significance of the trends and

correlations were assessed using a Monte-Carlo approach that generated 10,000 synthetic time series that share the same spectral characteristic as that of the underlying time series, thereby capturing any temporal autocorrelation[42,43]. The distribution of trends and/or correlations from the set of synthetic time series was then used to estimate the statistical significance of the actual result.

4. Modes of climate variability

The North Atlantic Oscillation (NAO), the difference in sea-level pressure between centers of action near Iceland and the Azores, is the leading mode of climate variability in the subpolar North Atlantic[44]. It has been argued to play a major role in modulating the intensity of oceanic convection in the Greenland Sea[45]. However, for the period of interest (1958-2014), the time series of Q_{thf}^{ocean} over both the Greenland and Iceland Seas are not significantly correlated with the winter mean NAO index[5] (-0.07 and -0.21, respectively). The relative strengths of the Icelandic Low and the Lofoten Low, a secondary regional circulation feature situated over the Norwegian Sea, has been shown to play an important role in the climate of the Nordic Seas[46]. The correlations of Q_{thf}^{ocean} with an index of the relative strength of these two circulation systems have substantially higher magnitudes for both gyres than those for the NAO (-0.24 and -0.49 respectively) and which are statistically significant at the 95th percentile confidence interval. This is consistent with previous work indicating that the relative strength of these two low-pressure systems modulates the magnitude of the air-sea fluxes over the Iceland Sea[47]. It also suggests, in agreement with previous studies[48,49], that modes of variability other than the NAO are needed to fully describe the climate in the region.

5. Oceanographic data

The geographical locations of the gyres in the Greenland and Iceland Seas were determined from the dynamic topography of the surface relative to 500 m using the NISE historical hydrographic database[50]. Broad minima reveal cyclonic gyres in the central Greenland and Iceland Seas. A closed contour of dynamic topography surrounding each minimum was chosen such that a sufficiently large number of homogeneous hydrographic profiles were contained within the region to obtain robust initial conditions for the mixed-layer model simulations. Most of the variability amongst the autumn profiles was inter-annual or spatial, which provides justification for using constant initial conditions for the mixed-layer model simulations.

6. Mixed-layer model details

The one-dimensional PWP[51] mixed-layer model has been shown to predict with skill the wintertime evolution of the mixed layer within similar cyclonic circulations[52]. To implement the model, fluxes of heat, freshwater, and momentum obtained from the ERA-I were imposed at the surface at each time step. The turbulent heat and longwave radiative fluxes provide the dominant contribution to the mixed-layer deepening[52]. The ERA-I has a well-documented ~20-30 W/m^2 bias in the longwave radiative flux at high latitudes[53,54] that was taken into account in the model's forcing. The model then adjusted the mixed-layer depth and properties until three stability criteria, involving the vertical density gradient and the bulk and gradient Richardson numbers, were satisfied. In light of the model's neglect of advection, as well as small-scale variability often present within a convective gyre, the agreement between the PWP model and the Argo floats in the

Iceland Sea for winters 2008 and 2012 is very good (Supp. Fig. 2). For these simulations the model was initialized by early November profiles from the floats in question and forced by 6-hourly atmospheric fluxes from the ERA-Interim reanalysis product.

The Greenland and Iceland Sea gyres have qualitatively different overall heat budgets. In the Greenland Sea the annual mean surface heat flux over the period 1980-2012 is large, 59W m^{-2}, while in the Iceland Sea it is very small, 10W m^{-2}. As such, lateral advection plays a more important role in the Greenland Sea gyre[55,56]. This was accounted for using the following parameterization. A continuous loss of 59W m^{-2} for the duration of one year corresponds to a temperature decrease of 0.45ºC over a 1000 m deep water column, which is a typical wintertime mixed-layer depth in the Greenland Sea based on Argo profiles made over the last decade. Assuming a constant rate of restratification throughout the year, a fixed amount of heat was added to the simulated temperature profile at each time step. This temperature increase was distributed throughout the water column such that the maximum temperature was near the surface (constant in the mixed layer, which was taken to be half of that inside the gyre), with an exponential decrease toward 1000 m. The shape closely resembles the difference between the mean temperature profiles within and just outside of the gyre (not shown). As Figure 4 demonstrates, with this approach the Greenland Sea simulations are in good agreement with the observed mixed-layer evolution as measured by Argo floats.

References

31 Uppala, S. M. *et al*. The ERA-40 re-analysis. *Quarterly Journal of the Royal Meteorological Society* **131**, 2961-3012, doi:10.1256/qj.04.176 (2005).

32 Dee, D. P. *et al*. The ERA-Interim reanalysis: configuration and performance of the data assimilation system. *Quarterly Journal of the Royal Meteorological Society* **137**, 553-597, doi:10.1002/qj.828 (2011).

33 Hein, P. F. & Brown, R. A. Observations of longitudinal roll vortices during arctic cold air outbreaks over open water. *Boundary-Layer Meteorology* **45**, 177-199, doi:10.1007/bf00120822 (1988).

34 Curry, J. A. *et al*. Seaflux. *Bulletin of the American Meteorological Society* **85**, 409-+, doi:10.1175/bams-85-3-409 (2004).

35 Renfrew, I. A. & Moore, G. W. K. An extreme cold-air outbreak over the Labrador Sea: Roll vortices and air-sea interaction. *Monthly Weather Review* **127**, 2379-2394, doi:10.1175/1520-0493(1999)127<2379:aecaoo>2.0.co;2 (1999).

36 Brummer, B. Boundary-layer modification in wintertime cold-air outbreaks from the arctic sea ice. *Boundary-Layer Meteorology* **80**, 109-125, doi:10.1007/bf00119014 (1996).

37 Petersen, G. N. & Renfrew, I. A. Aircraft-based observations of air-sea fluxes over Denmark Strait and the Irminger Sea during high wind speed conditions. *Quarterly Journal of the Royal Meteorological Society* **135**, 2030-2045, doi:10.1002/qj.355 (2009).

38 ECMWF. IFS DOCUMENTATION – Cy40r1. (2013).

39 Bourassa, M. A. *et al*. High-latitude ocean and sea ice surface fluxes: Challenges for climate research. *Bulletin of the American Meteorological Society* **94**, 403-423, doi:10.1175/bams-d-11-00244.1 (2013).

40 Gilman, D. L., Fuglister, F. J. & Mitchell, J. M. On the Power Spectrum of "Red Noise". *Journal of the Atmospheric Sciences* **20**, 182-184, doi:10.1175/1520-0469(1963)020<0182:OTPSON>2.0.CO;2 (1963).

41 Allen, M. R. & Smith, L. A. Monte Carlo SSA: Detecting irregular oscillations in the presence of colored noise. *Journal of Climate* **9**, 3373-3404 (1996).

42 Moore, G. W. K. Surface pressure record of Tibetan Plateau warming since the 1870s. *Quarterly Journal of the Royal Meteorological Society* **138**, 1999-2008, doi:10.1002/qj.1948 (2012).

43 Rudnick, D. L. & Davis, R. E. Red noise and regime shifts. *Deep-Sea Research Part I-Oceanographic Research Papers* **50**, 691-699, doi:10.1016/s0967-0637(03)00053-0 (2003).

44 Hurrell, J. W. Decadal trends in the North-Atlantic Oscillation - regional temperatures and precipitation. *Science* **269**, 676-679, doi:10.1126/science.269.5224.676 (1995).

45 Dickson, B. From the Labrador Sea to global change. *Nature* **386**, 649-650, doi:10.1038/386649a0 (1997).

46 Jahnke-Bornemann, A. & Bruemmer, B. The Iceland-Lofotes pressure difference: different states of the North Atlantic low-pressure zone. *Tellus Series a-Dynamic Meteorology and Oceanography* **61**, 466-475, doi:10.1111/j.1600-0870.2009.00401.x (2009).

47 Moore, G. W. K., Renfrew, I. A. & Pickart, R. S. Spatial distribution of air-sea heat fluxes over the sub-polar North Atlantic Ocean. *Geophysical Research Letters* **39**, doi:10.1029/2012gl053097 (2012).

48 Moore, G. W. K., Renfrew, I. A. & Pickart, R. S. Multidecadal Mobility of the North Atlantic Oscillation. *Journal of Climate* **26**, 2453-2466, doi:10.1175/jcli-d-12-00023.1 (2013).

49 Kelly, P. M., Goodess, C. M. & Cherry, B. S. G. The interpretation of the Icelandic sea ice record. *Journal of Geophysical Research-Oceans* **92**, 10835-10843, doi:10.1029/JC092iC10p10835 (1987).

50 Nilsen, J. E. Ø., Hatun, H., Mork, K. A. & Valdimarsson, H. The NISE data set., (Faroese Fisheries Laboratory, Torshavn, Faroe Islands, 2008).

51 Price, J. F., Weller, R. A. & Pinkel, R. Diurnal cycling: Observations and models of the upper ocean response to diurnal heating, cooling, and wind mixing. *Journal of Geophysical Research-Atmospheres* **91**, 8411–8427 (1986).

52 Våge, K., Pickart, R. S., Moore, G. W. K. & Ribergaard, M. H. Winter mixed-layer development in the central Irminger Sea: The effect of strong, intermittent wind events. *Journal of Physical Oceanography* **38**, 541–565 (2008).

53 Chaudhuri, A. H., Ponte, R. M. & Nguyen, A. T. A Comparison of Atmospheric Reanalysis Products for the Arctic Ocean and Implications for Uncertainties in Air-Sea Fluxes. *Journal of Climate* **27**, 5411-5421, doi:10.1175/jcli-d-13-00424.1 (2014).

54 Walsh, J. E., Chapman, W. L. & Portis, D. H. Arctic Cloud Fraction and Radiative Fluxes in Atmospheric Reanalyses. *Journal of Climate* **22**, 2316-2334, doi:10.1175/2008jcli2213.1 (2009).

55 Large, W. G., McWilliams, J. C. & Doney, S. C. Oceanic vertical mixing - a review and a model with a nonlocal boundary-layer parameterization. *Reviews of Geophysics* **32**, 363-403, doi:10.1029/94rg01872 (1994).

56 Latarius, K. & Quadfasel, D. Seasonal to inter-annual variability of temperature and salinity in the Greenland Sea Gyre: heat and freshwater budgets. *Tellus Series a-Dynamic Meteorology and Oceanography* **62**, 497-515, doi:10.1111/j.1600-0870.2010.00453.x (2010).

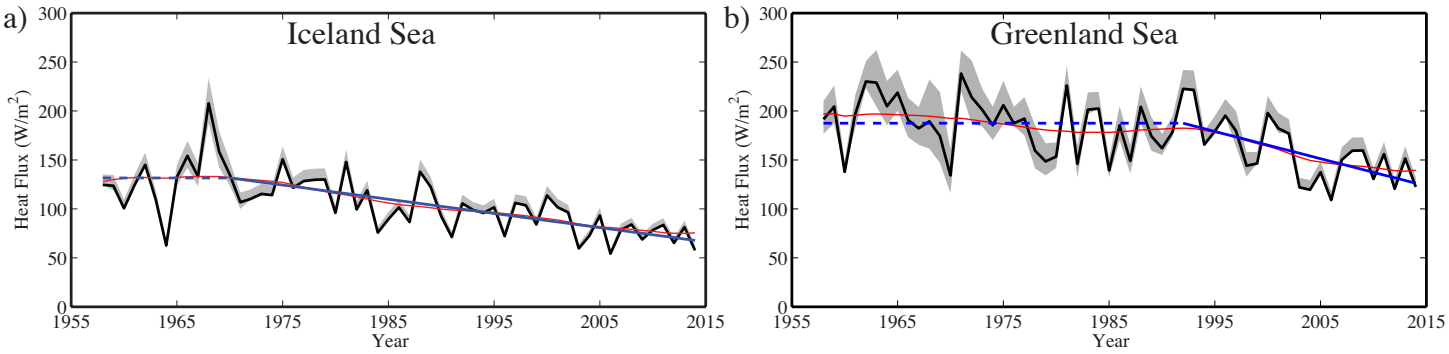

Supplementary Figure 1) Time series of the winter mean total open ocean heat flux over the Iceland and Greenland Sea gyres. Panels (a) and (b) show the open ocean total heat flux (W m^{-2}) with the shading representative of the uncertainty associated with the sea-ice concentration. The red curves are from the SSA reconstructions of the low frequency variability in the time series, while the blue lines are continuous piecewise linear least squares fits with breakpoints prescribed by the character of the respective SSA reconstructions. The trend lines that are solid are statistically significant at the 95% confidence level using a test that takes into account the reduced degrees of freedom that are the result of the autocorrelation or 'red noise' characteristic of geophysical time series. See Figure 1 for the location of the gyres.

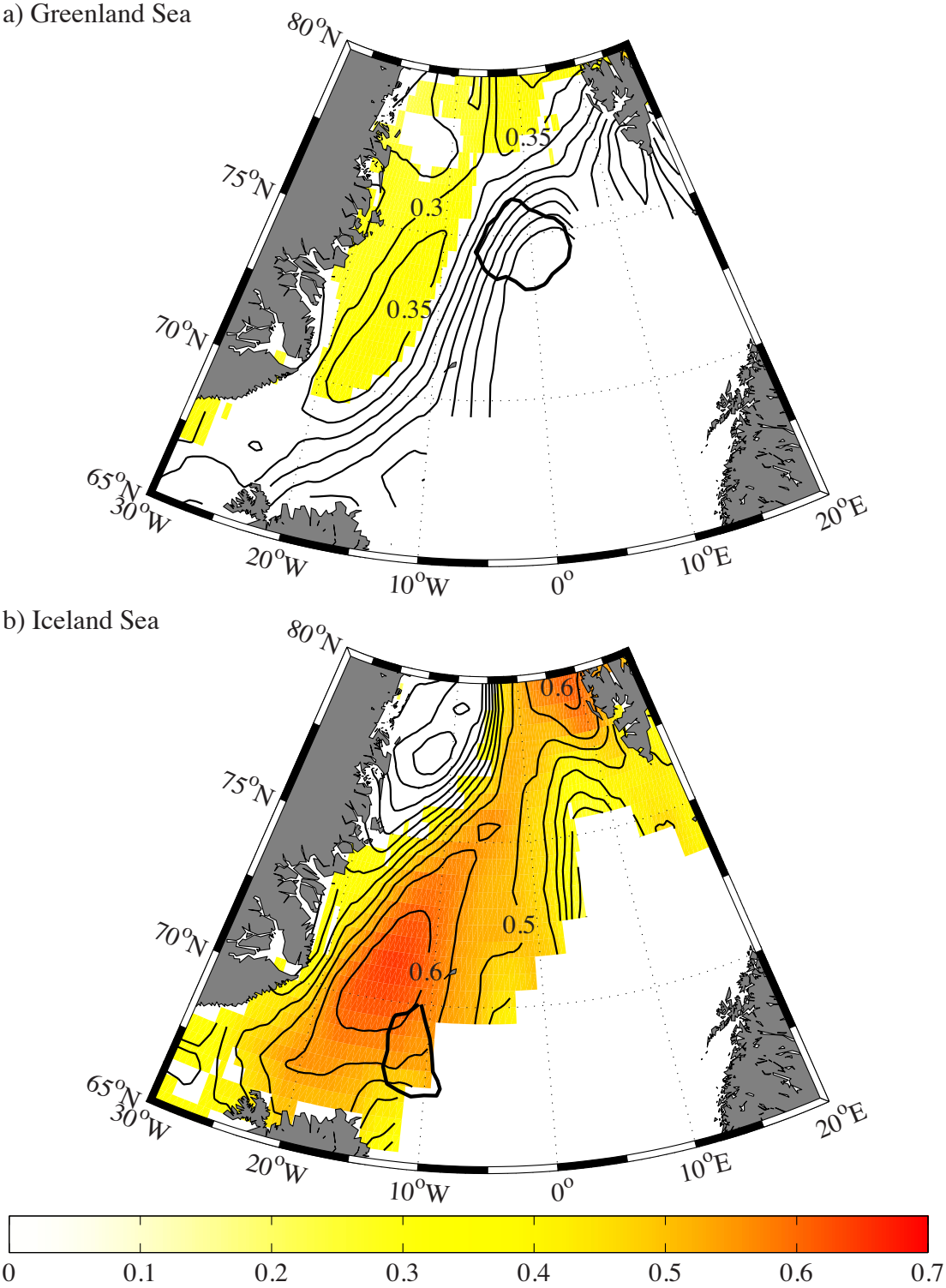

Supplementary Figure 2) Spatial correlation of the winter mean sea ice concentration field with the winter mean open ocean total heat flux over each gyre. Panels are for a) the Greenland Sea and b) the Iceland Sea. The locations of the Iceland and Greenland Sea gyres are indicated in the respective panel by the thick black curve. Shading represents the regions where the correlation is statistically significant at the 95% confidence interval.

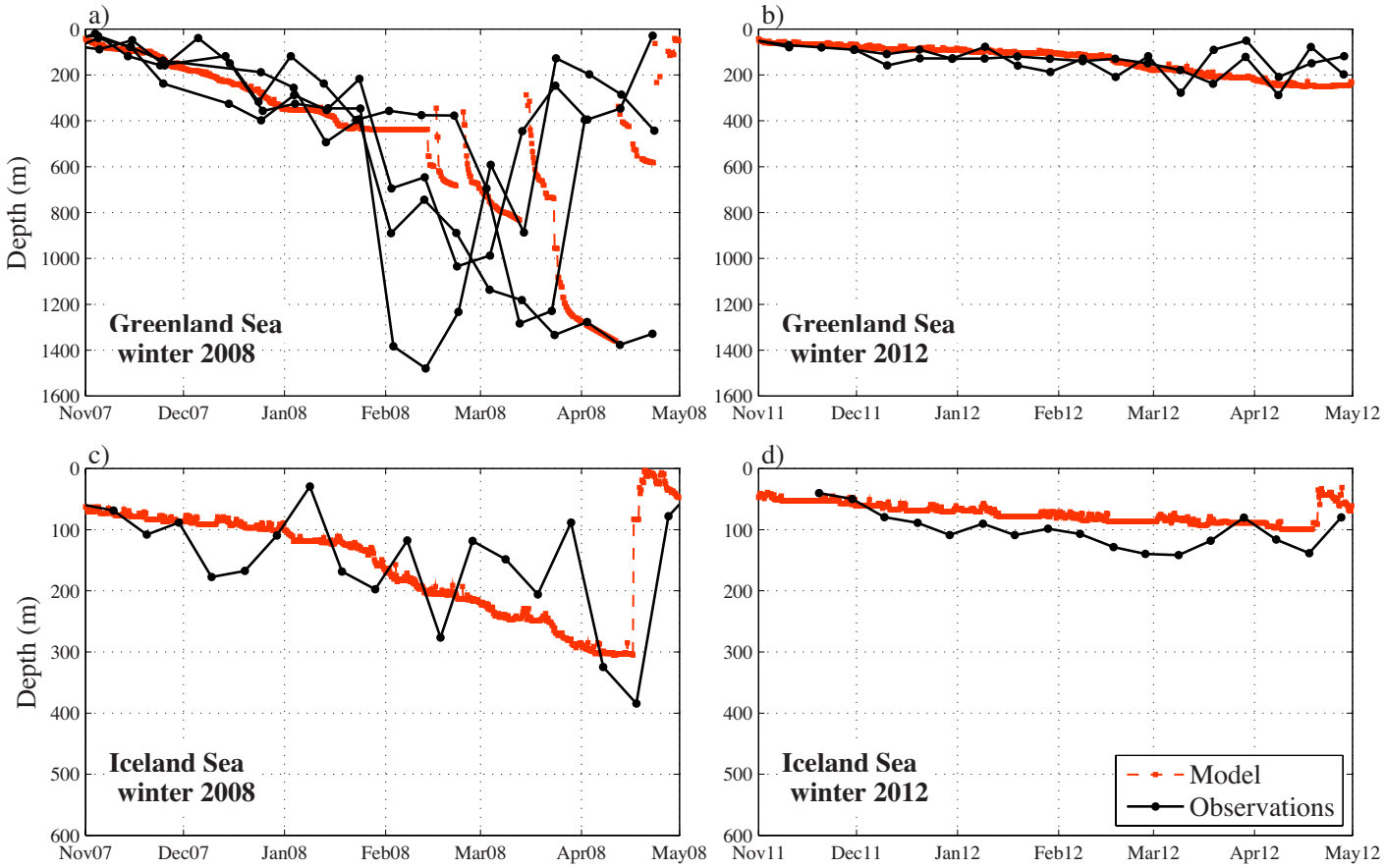

Supplementary Figure 3) Simulated and observed wintertime evolution of the mixed layers in the Greenland Sea and Iceland Sea gyres for winters 2008 and 2012. Mixed-layer depths are shown as red lines (simulated) and black crosses (observations from Argo floats). The upper row shows the Greenland Sea gyre and the lower row shows the Iceland Sea gyre. The left column is winter 2008 and the right column is winter 2012. Note the difference in vertical scale between the upper and lower rows.